Fabrication of High Performance CdZnTe Quasi-Hemispherical Gamma-ray CAPture™ Plus Detectors

Csaba Szeles, Derek Bale, Joseph Grosholz, Jr., Gary L. Smith, Michael Blostein, and John Eger

eV PRODUCTS a division of II-VI, Inc., Saxonburg, PA 16056

ABSTRACT

We report on the material selection, testing and fabrication technology development of high performance CdZnTe quasi-hemispherical CAPture™ Plus radiation detectors. Quasi-hemispherical CdZnTe detectors offer a cost effective alternative to other single-polarity (electron-only) detector configurations such as co-planar grid, pixilated or Frisch ring CdZnTe detectors with comparable energy resolution both in the high (>500 keV) and low energy range (<500 keV). The performance of the quasi-hemispherical detectors is controlled by charge transport properties of the CdZnTe crystals, quality of device fabrication and device integration. Similarly to other single-polarity CdZnTe device configurations the charge transport uniformity of the CdZnTe crystals is critical for achieving high energy resolution. We realized this by carefully selecting high electron transport CdZnTe crystals ($\mu\tau_e \geq 6.0\times10^{-3}$ cm^2/V) with uniform distribution of structural defects. Infra-red microscopy was employed for structural defect mapping of the crystals. Low sub-surface damage state-of-the art multi- and single-wire saw technologies were used to slice and dice the single crystal detector elements out of the CdZnTe ingots. Dimensional control of the crystals was preserved throughout chemical etching and chemo-mechanical polishing by minimizing material removal. Device fabrication employing state-of-the art photolithography, electrode deposition and surface passivation enabled the application of bias voltages as high as 5000 V/cm on the devices. With carefully selected high uniformity CdZnTe crystals and low-noise preamplifier energy resolution better than 4.8% FWHM at 81 keV, 3.0% FWHM at 122 keV and 1.5% FWHM at 662 keV was achieved on 10×10×5 mm^3 quasi-hemispherical detectors.

Keywords: Cadmium Zinc Telluride, CdZnTe, nuclear radiation detectors, quasi-hemispherical detectors, x-ray and γ-ray spectroscopy

1. INTRODUCTION

The physical properties of semi-insulating (SI) Cadmium Zinc Telluride (CdZnTe) such as high atomic number, high density, wide band gap, low chemical reactivity and long term stability make it an excellent material candidate for high efficiency, high-resolution room-temperature nuclear radiation detectors. Intense research of crystal growth and electrical compensation in CdZnTe in the last 10-15 years led to developments that allow the growth of SI CdZnTe crystals with low defect density and very good charge transport properties. Today, SI CdZnTe crystals are available commercially and the CdZnTe-based room-temperature radiation detectors and detector arrays are steadily gaining acceptance in many medical, industrial, security, safeguards and scientific X-ray and γ-ray imaging and spectroscopic applications.[1]

While CdZnTe crystals are readily available for simpler counting and monitoring applications, large field-of-view imaging and high-sensitivity, high-resolution spectroscopic applications demand larger and more uniform CdZnTe single crystals with better charge transport properties. The electron mobility-lifetime product ($\mu\tau_e$) of CdZnTe crystals grown by the high-pressure electro-dynamic gradient freeze (HP EDGF)[2], conventional vertical Bridgman[3] and traveling heater method (THM)[4] have steadily climbed from the low 10^{-3} cm^2/V range to the 10^{-2} cm^2/V range in recent years. On the other hand the growth of SI CdZnTe *single crystals*, with spatially uniform charge transport properties that are required for these applications remains a challenge due to the inherent complexity of the crystallization and defect formation processes in these crystals.[5,6]

High performance spectroscopic CdZnTe detectors such as the 3D depth sensing position sensitive (3D DSPS) devices[7], and co-planar grid (CPG) detectors[8] require the highest electron transport and uniformity single crystals to achieve the best possible energy resolution. In order to maximize fabrication and testing yields and minimize fabrication costs of these detectors the CdZnTe single crystals have to be carefully mined from the ingots and fully characterized in the early stage of the fabrication process. This is only possible by carefully designed *material selection, crystal mining* and *characterization* process that ensures high testing yields of the fully fabricated and integrated detectors.

Hard X-Ray and Gamma-Ray Detector Physics VIII, edited by Larry A. Franks, Arnold Burger,
Ralph B. James, Proceedings of SPIE Vol. 6319 (SPIE, Bellingham, WA, 2006)

191

Commercial suppliers of SI CdZnTe crystals and detectors are faced with a yield optimization problem. It is important to harvest single crystals from CdZnTe ingots (boules) at a maximum yield and then to allocate the harvested crystals to the various detector products in such a way to maximize the fabrication and testing yields of each detector product in their portfolio. Without this approach it is difficult to minimize the crystal mining, fabrication, integration and testing costs and provide CdZnTe crystals and detectors at affordable prices.

The same CdZnTe single crystal can be fabricated into 3D DSPS, CPG or simpler Frisch ring or quasi-hemispherical spectroscopic detectors. In order to achieve their maximum performance 3D DSPS and CPG detectors require premium quality high electron transport and excellent uniformity single crystals. In addition, the readout electronics and integration cost of these devices is relatively high. In particular the 3D DSPS detectors require 100+ readout channels and significant computational overhead to perform the depth and multiple-interaction corrections. Because of the high manufacturing costs it is not logical to fabricate 3D DSPS and CPG detectors from lower quality CdZnTe crystals. In contrast Frisch ring and quasi-hemispherical devices require only a single readout channel and potentially can be produced at lower cost. It is important to develop an understanding of the performance and fabrication cost tradeoffs of these detector configurations and develop the CdZnTe crystal performance requirements to achieve a given target performance of such detectors.

In this paper, we evaluated the material performance requirements of quasi-hemispherical CdZnTe radiation detectors and developed a prototype fabrication process. It was established that the performance of these detectors is controlled by the charge transport uniformity of the crystals. We have demonstrated energy resolution of 1.5–3.5% FWHM at 662 keV depending on the uniformity of the crystals. It was also established that the costs of these devices is dominated by the yield of the single crystals. Because the yield of premium quality crystals is limited, the manufacturing costs of high-resolution (1.5–1.8% FWHM) CAPture™ Plus radiation detectors is also high. In contrast single crystals of lesser uniformity are readily available and lower energy resolution (2.5–3.5% FWHM) CAPture™ Plus detectors can be manufactured at lower costs.

In the following sections we will review the detector design, fabrication and testing process developed and successfully implemented at eV PRODUCTS for all higher performance spectroscopic detectors. The flow chart of the process is shown in Fig.1. The process starts with device design using the powerful eVDSIM detector design tool.[9] The device simulation provides the material selection criteria i.e. electron and hole mobility-lifetime product ranges optimal for the given detector configuration. In the next step CdZnTe wafers are sliced from ingots exhibiting appropriate charge transport properties. This is followed by the mining of single crystal detector elements with uniform distribution of Te inclusions. Finally the selected crystals are fabricated and integrated into radiation detectors to meet the targeted performance criteria.
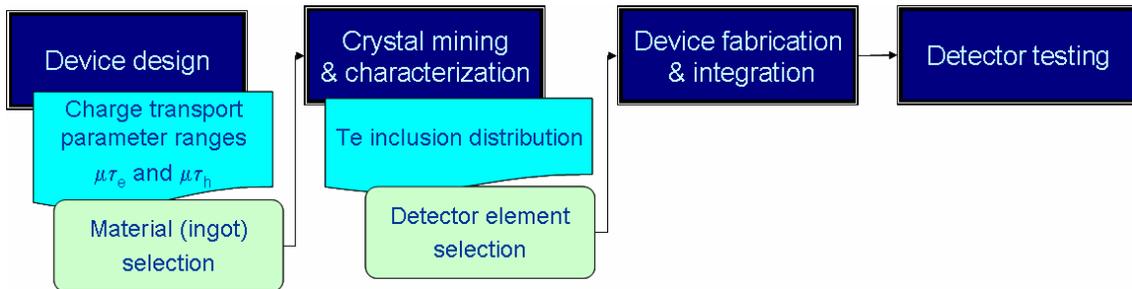

Fig. 1.   Flow diagram of the detector design, fabrication and testing process.

2. DETECTOR DESIGN CRITERIA

The design parameters of quasi-hemispherical CdZnTe detectors are the physical dimensions (x, y, z), the pixel diameter (d), bias voltage (V), and the electron and hole mobility lifetime products ($\mu\tau_e$ and $\mu\tau_h$), respectively. The quasi-hemispherical design sets the $x/z = y/z = 2$ ratios. The photon energy range and desired detection efficiency dictates the choice of the thickness (z) and the corresponding electron transport ($\mu\tau_e$). In order to maintain the same trapping probability and same electric field an increasing thickness requires a proportional increase of the electron mobility-lifetime product.[10] A simple $\mu\tau_e$ estimate based on the charge collection calculated by eVDSIM is given in Table I.

It was clearly established using eVDSIM modeling that the first order dominant parameters controlling the performance of quasi-hemispherical detectors are the electron transport ($\mu\tau_e$) and the bias voltage (V). Low electron transport material or an under-biased condition severely deteriorates the performance of the device. It was also established that the pixel size (d)

and hole transport ($\mu\tau_h$) are second order parameters and have lesser influence on the performance of the device. We will show later that the charge transport uniformity of the detector crystals plays a major role in the performance of the device.

Fig. 2. Quasi-hemispherical CdZnTe detector configuration.

Table I.

z (mm)	$\mu\tau_e$ (cm^2/V)
5	3×10^{-3}
10	6×10^{-3}
15	9×10^{-3}

3. CdZnTe CRYSTAL GROWTH

eV PRODUCTS uses the high-pressure electro-dynamic gradient freeze (HP EDGF) crystal growth technique to grow the semi-insulating detector grade CdZnTe ingots. Currently we operate two generations of this technology. The Gen-3+ HP EDGF produces 12-kg 5.5" (~140 mm) diameter ingots while the recently introduced fifth generation Gen-5 HP EDGF technology produces 24-kg 8.0" (~200 mm) diameter ingots (Fig. 3).
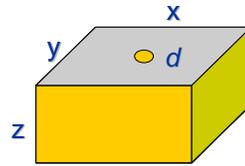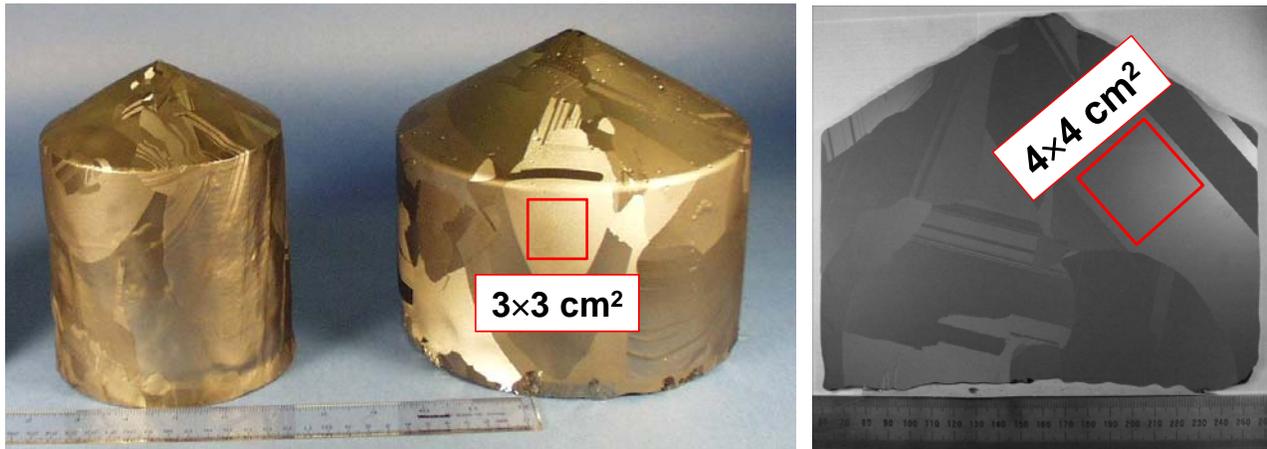

Fig. 3. Comparison of the 5.5"-diameter and 8.0"-diameter CdZnTe ingots grown by the Gen-3+ and Gen-5 HP EDGF crystal growth systems, respectively. The right pane shows an axial slice of a Gen-5 8.0"-diameter CdZnTe ingot.

The primary challenges of CdZnTe crystal growth are a) reliable electrical compensation techniques to reproducibly obtain fully compensated high-resistivity ingots with good charge transport properties, b) growth of sufficiently large single crystals with sufficiently high yield, and c) growth of single crystals with uniform charge transport properties. It is now unambiguously established that Te inclusions distributed uniformly in the single crystals, forming spatially correlated clusters or decorating twin planes are the primary defects hampering the charge transport uniformity of CdZnTe
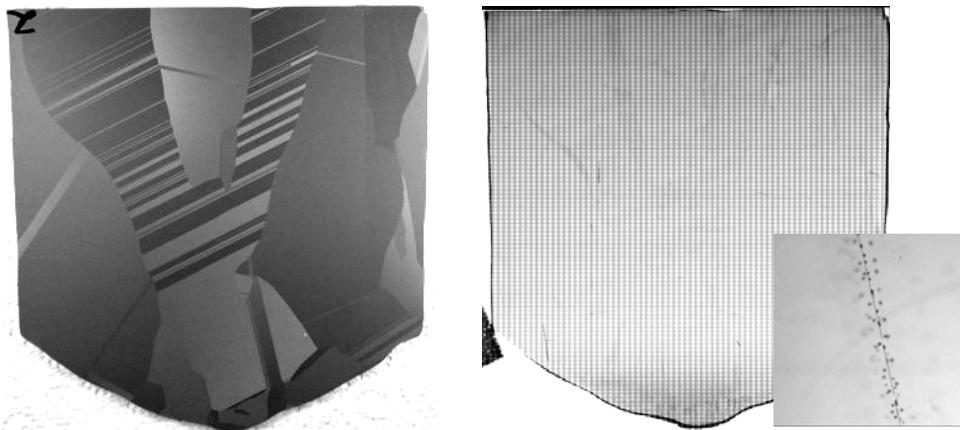

Fig. 4. An axial slice from a 5.5"-diameter CdZnTe ingot grown by the Gen-3+ HP EDGF technology. The right pane shows the IR microscopy map of the slice. Te inclusions of 25–35 μm average diameter decorate the various structural defects such as grain and twin boundaries. An enlarged view of a Te-inclusion decorated twin plane is shown in the inset.

crystals.[8,11,12] Fig. 4 shows an axial slice from a 5.5"-diamter CdZnTe ingot grown by the Gen-3+ HP EDGF technology. The right pane shows the IR microscopy map of the slice. Te inclusions of 25–35 μm average diameter decorate the various structural defects such as grain and twin boundaries. An enlarged view of a Te-inclusion decorated twin plane is shown in the inset.

4. MATERIAL SELECTION AND CRYSTAL MINING

Because the electron mobility-lifetime product is the primary dominant material property controlling the performance of quasi-hemispherical CdZnTe detectors we first have to select material from ingots with sufficiently high $\mu\tau_e$ for the given thickness of the device. eV PRODUCTS characterizes both the axial and radial spatial distribution of charge transport properties ($\mu\tau_e$ and resistivity) of the as-grown CdZnTe ingots. For the axial distribution $5\times5\times2$ mm^3 samples are cut along the centerline of the axial slice as shown in Fig. 5. The samples are fabricated into planar detector devices to measure the
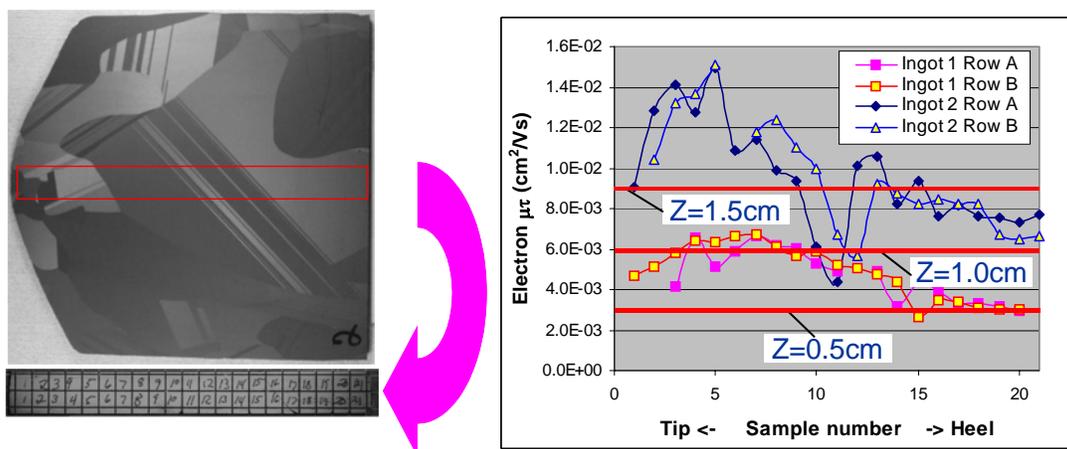

Fig. 5. $5\times5\times2$ mm^3 samples cut along the centerline of a Gen-3+ HP EDGF CdZnTe ingot for electrical characterization (left pane). Axial distribution of $\mu\tau_e$ in two different CdZnTe ingots (right pane). The figure also shows the required $\mu\tau_e$ for three different device thicknesses and illustrates that the availability of CdZnTe crystals reduces with increasing $\mu\tau_e$.
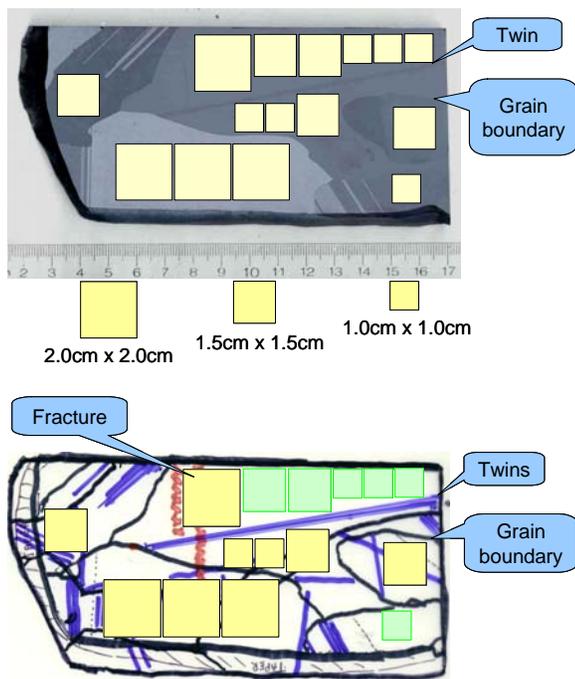

Fig. 6. Mapping of single crystal detector elements free of correlated Te-inclusion clusters and other structural defects using IR microscopy.

resistivity[13] and $\mu\tau_e$. For the later the voltage dependence of the 5.5 MeV photopeak from a ^{241}Am alpha source is measured and fitted to the Hecht model.[14] Fig. 5 also shows the required $\mu\tau_e$ for three different device thicknesses and illustrates that the availability of CdZnTe crystals reduces with increasing $\mu\tau_e$.

Once CdZnTe ingot sections with sufficiently high electron transport properties are selected material slices are cut to the
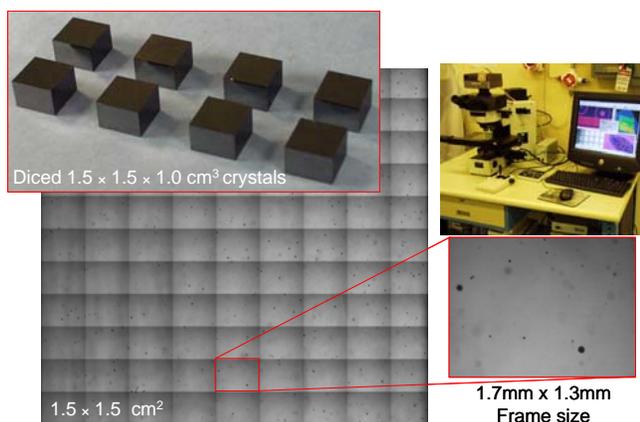

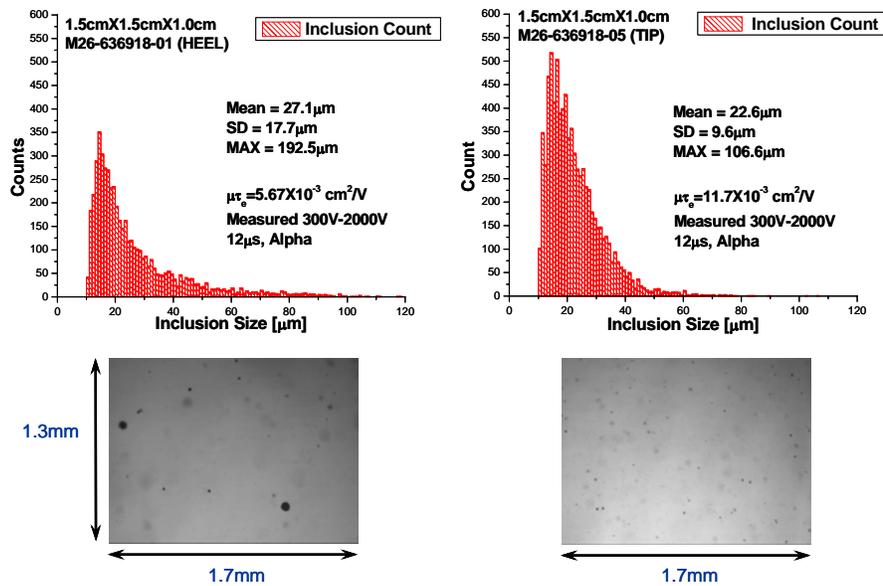**Fig. 7.** IR microscopy mapping of single crystal detector elements.

Fig. 8. The size distribution of Te inclusions in two CdZnTe single crystals measured using IR microscopy mapping.

design thickness (z) using a low-damage, high-precision multi-wire saw (MWS) or a single-wire saw (SWS). In the next step potential single crystal areas are mapped for the various device sizes. The top pane of Fig. 6 shows an axial slice mapped for three different device dimensions. In the next step the material slice is polished and inspected under an infra-red (IR) microscope to identify Te-inclusion decorated grain boundaries, twin planes and fractures that penetrate the single crystal areas. The IR microscopy mapping is used to identify the single crystal areas free of these defects. The bottom pane of Fig. 6 illustrates that after IR microscopy mapping only a smaller fraction of the single crystal areas are available to mine out detector elements free from correlated clusters of Te inclusions.

In the next step the single crystal detector elements are mined from the slices using SWS dicing (Fig. 7). The detector crystals are then carefully mapped with a higher resolution IR microscope to verify the absence of decorated grain boundaries, twin planes or other correlated Te-inclusion clusters and to measure the size distribution of Te inclusions in the crystals. Typical results are shown in Fig. 8. Here we compare the size distribution of Te inclusions in two different $1.5 \times 1.5 \times 1.0$ cm^3 CdZnTe single crystals. The crystal in the left pane has fewer but on average larger diameter Te inclusions. The size distribution in this crystal also shows a long tail indicating the presence of a few large (>60 μm diameter) Te inclusions.

5. DEVICE FABRICATION AND MODULE ASSEMBLY

In order to minimize the manufacturing costs the $10 \times 10 \times 5$ mm^3 CdZnTe single crystals were processed using a relatively simple fabrication process. First the crystals were etched in a Br solution to remove a 100-μm thick layer from the surface in order to eliminate the surface and subsurface saw damage introduced during slicing and dicing. The low-damage high-precision wire saw slicing and dicing enabled this relatively small material removal. In contrast blade slicing and dicing typically introduces saw damage much deeper into the crystals and several hundred microns of material removal is needed to fully eliminate this performance degrading damage layer.[15] There are numerous choices for the Br solution chemistry for etching CdZnTe crystals such as methanol, ethanol, ethylene glycol and others. Br solutions tend to be very aggressive and produce fast material removal rates. However, such aggressive etch chemistry also leaves the surface uneven with wavy or orange peel morphology. More importantly they cause excessive edge and corner rounding and with such processes it is difficult to maintain dimensional control of the crystals. With appropriate choice of the etch chemistry, concentrations, Ph, temperature, and agitation much improved uniform removal rates are achievable. We have developed and implemented such a process and reproducibly achieving edge rounding with less than 50 μm radius and surface waviness less than 5 μm.

Electrode deposition was performed using DC sputtering. We chose to employ 1000Å/1000Å Pt/Au double layer electrodes for both the cathode and the anode in order to make the electrodes robust and resistant to damage during the downstream handling during fabrication and integration. First the cathode electrode was deposited on 5 etched surfaces of the crystal to form the cup-shape electrode. In order to protect this electrode during further processing it was spray coated

with a protective coating. In the next step the anode surface was chemo-mechanically polished (CMP). It is to be noted that because of the excellent dimensional accuracy of both the wire saw technology (better than 16 μm total thickness variation across an 8" diameter ingot) and chemical etching, there is no need for stock removal with mechanical polishing. Our two-
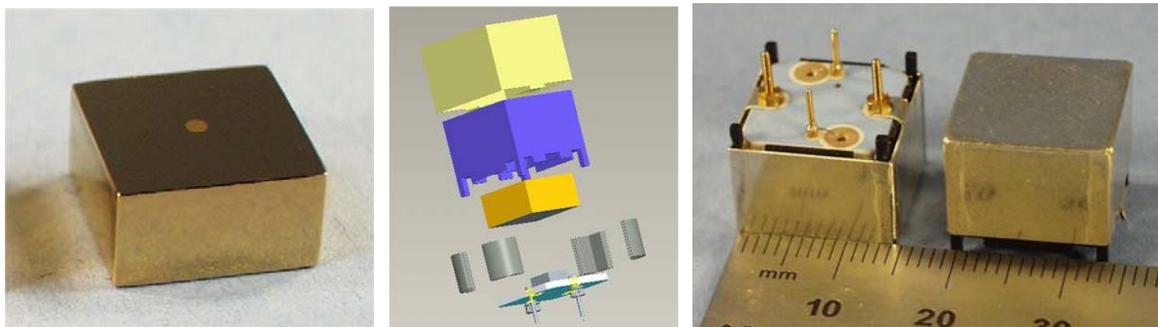

Fig. 9.   Quasi-hemispherical CdZnTe detector element and the CAPture™ Plus radiation detector module.

step CMP process, with less than 5 μm material removal, produces excellent results.

Photolithography was used to define the size of the pixel during the anode deposition. A passivation layer was deposited on the exposed anode CdZnTe surface. The surface passivation is critical to enable the application of sufficiently high bias voltage across the anode surface without premature breakdown. With our passivation technology we are now achieving 5000 V/cm bias without breakdown. We also apply an encapsulation layer to the passivation layer in order to protect it from damage during detector integration and ensure the long term stability of the device. Fig. 9 shows an example of a $10 \times 10 \times 5$ mm^3 quasi-hemispherical detector before integration.

The detector is bonded to a plastic cup to ensure mechanical stability. Lead wires are attached to the electrodes with silver epoxy bonds. The wires are connected to connector pins at opposite side of the substrate where the bias voltage is applied. The detector-substrate assembly is encapsulated in an electromagnetic shield as shown in Fig. 9. The CAPture™ Plus detector module can be used as a stand alone detector with appropriate low noise readout electronics or can be integrated into multi-detector systems.

6. PERFORMANCE CHARACTERIZATION

Fig. 10 shows the room-temperature response of a $10 \times 10 \times 5$ mm^3 quasi-hemispherical CAPture™ Plus CdZnTe detector to ^{133}Ba, ^{57}Co and ^{137}Cs radiation. All measurements were taken at 1500 V bias and 1 μs shaping tame utilizing the eV-550 preamplifier. The full width half maximum (FWHM) energy resolution of the device is 4.86% @ 81 keV, 3.12% @ 122 keV and 1.57% @ 662 keV. The peak to Compton ratio at 662 keV is 6.4 for this device. Typical for quasi-hemispherical detectors the photo-peaks show a low-energy tailing. Obviously this is the result of incomplete charge collection as this device configuration cannot fully compensate for the depth-dependent signal amplitude caused by hole trapping. This device that was fabricated from a CdZnTe crystal having $\mu\tau_e = 9.0 \times 10^{-3}$ cm^2/V shows a performance as good as or better than what was predicted by the device simulation.

The correlation between the model prediction and experimental result is however not always satisfactory. In Fig. 11 we compare the simulated and measured FWHM energy resolution of 27 quasi-hemispherical detectors as a function of electron mobility lifetime product and applied bias. All measurements were taken at 1500 V bias. It is clear from Fig. 11 that a significant fraction of the measured energy resolutions is worse than predicted. Based on earlier studies of performance deterioration of both 3D DSPS and CPG detectors we suspect that the energy resolution degradation of quasi-hemispherical devices is also caused by Te inclusions in the crystals. In order to investigate this hypothesis we analyzed the Te inclusion size distribution in five (5) crystals with similar electron transport properties $\mu\tau_e = (1.1 \pm 0.1) \times 10^{-2}$ cm^2/V as shown in Fig. 12. Table II compares the FWHM energy resolution at 662 keV and the total Te-inclusion surface area found by IR microscopy mapping. While the correlation is not compelling it is noteworthy that the best energy resolution is obtained on a detector crystal containing the least amount of Te inclusions. Recent results by Bolotnikov, Carini and Camarda from BNL show a strong correlation between the size of the Te inclusions and the energy resolution of CdZnTe Frisch ring detectors.[16] The 5 detectors studied here all show a fairly similar average diameter and their size distribution is also similar as shown in Fig. 12.

Fig. 13 shows the time evolution of the FWHM energy resolution at 662 keV in a period of 20 hours for three different quasi-hemispherical detectors. Detector #3 with the best initial resolution of about 2.0% shows only a minor deterioration to 2.1%. In contrast the two detectors (#1 and #4) with about 3.0% starting resolution undergo a steady deterioration to 3.5% and 3.8% within 10 hours. Fig. 13 also shows the IR microscopy image of two detectors. Detector #3 with better energy resolution and lesser temporal variation contains much smaller size Te inclusions (~15 μm). In contrast detector #1 with worse energy resolution and strong temporal deterioration contains larger size Te inclusions (~35 μm).
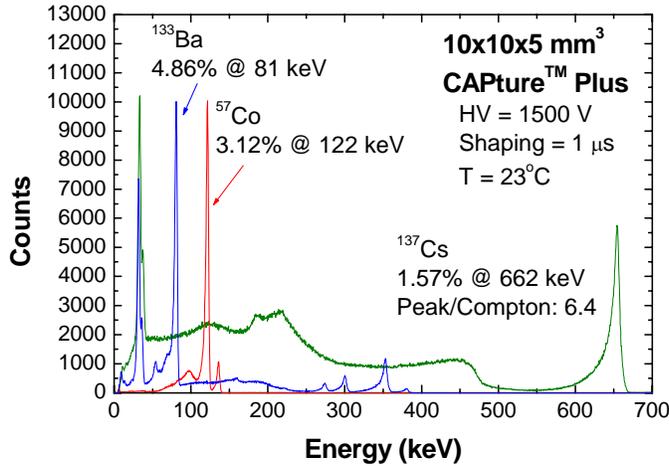

Fig. 10. The room-temperature response of a $10\times10\times5$ mm^3 quasi-hemispherical CAPture™ Plus CdZnTe detector to ^{133}Ba, ^{57}Co and ^{137}Cs radiation.
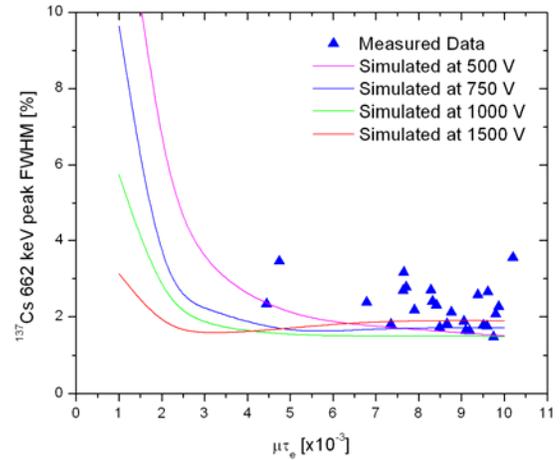
Fig. 11. Simulated and measured FWHM energy resolution @ 662 keV of 27 quasi-hemispherical detectors as a function of $\mu\tau_e$ and applied bias

It is to be noted that the long time scales of the energy resolution deterioration shown in Fig. 13 is inconsistent with trapping and detrapping phenomena that occur much faster at much shorter time scales. Such long timescales are rather characteristic of macroscopic charging phenomena. We suspect that the phenomenon is associated with the charging of Te inclusions which in turn lead to enhanced electron tapping or recombination on Te inclusions and the deterioration of the energy resolution. This model is consistent with our charge transport simulations that show that the electric field is lower in 90% of the volume of quasi-hemispherical detectors than in planar detectors. The low electric field and slow drift speed of carriers in this region increases the trapping probability of electrons and holes. We are currently evaluating the validity of the Te inclusion charging hypothesis and will publish the results in a separate publication.
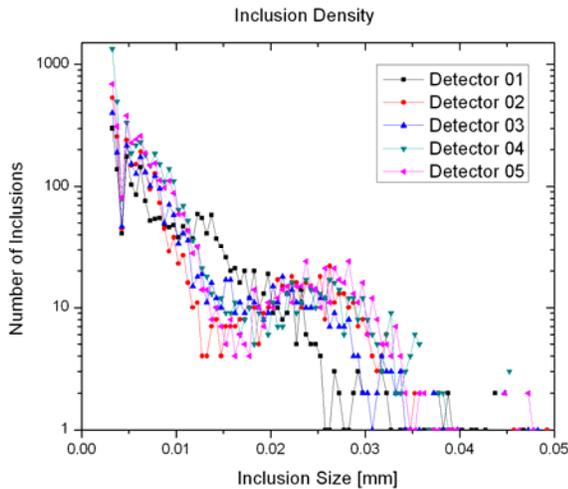

Table II.

Detector	Electron $\mu\tau$ [cm^2/V]	Initial Resolution [%] @ 662 keV	Te Inclusion Area [mm^2]
1	1.2×10^{-2}	3.12	2.56
2	1.1×10^{-2}	3.15	2.47
3	1.0×10^{-2}	2.01	2.38
4	1.2×10^{-2}	3.02	3.34
5	1.1×10^{-2}	3.09	3.56

Fig. 12. The Te-inclusion size distribution in five $10\times10\times5$ mm^3 CdZnTe crystals. The $\mu\tau_e$ of the crystals and performance of the fabricated quasi-hemispherical detectors are summarized in Table II.
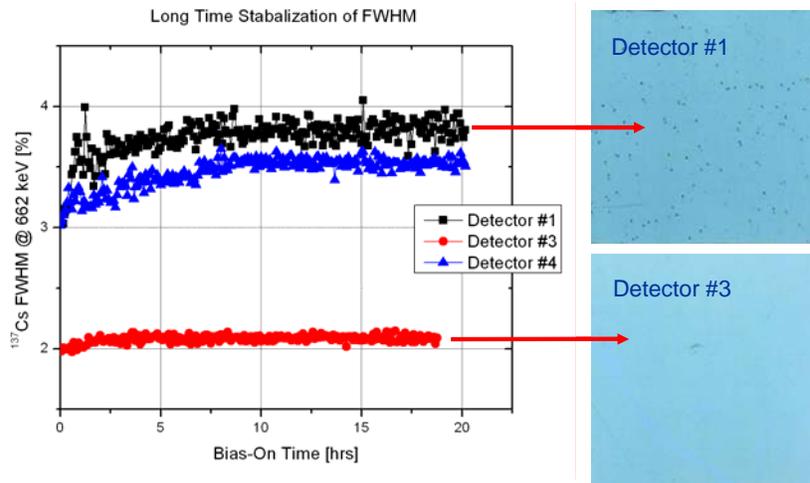
Fig. 13. Time dependence of the FWHM energy resolution at 662 keV for three different quasi-hemispherical detectors with different Te inclusion size distribution. The IR microscopy image in the right illustrates the Te inclusions sizes.

Sample #3 in Fig. 13 shows that with appropriate choice of the CdZnTe crystal the energy-resolution deterioration can be nearly completely eliminated in CAPture™ Plus detectors. The results so far indicate that for CdZnTe crystals with small diameter (≥15 μm) uniformly distributed Te inclusions the long-term resolution deterioration is less than 5%.

4. CONCLUSIONS

In this study we evaluated the feasibility of developing a fabrication technology for the low-cost manufacture of high performance CdZnTe quasi-hemispherical gamma-ray CAPture™ Plus detectors. It was found that the performance and stability of the detectors is dominated by the quality of the crystals. The results suggest that the primary performance and stability limiting defects are Te inclusions. This is consistent with results obtained for 3D DSPS, CPG and other CdZnTe detectors. The manufacturing cost of CAPture™ Plus detectors is dominated by the yield and availability of high-quality CdZnTe single crystals. With carefully selected high uniformity and high electron transport ($\mu\tau_e \geq 6.0\times10^{-3}$ cm^2/V) CdZnTe single crystals and low-noise preamplifier, energy resolution better than 4.8% FWHM at 81 keV, 3.0% FWHM at 122 keV and 1.5% FWHM at 662 keV is achievable for $10\times10\times5$ mm^3 quasi-hemispherical detectors.

REFERENCES

[1] T.E. Schlesinger, J.E. Toney, H. Yoon, E.Y. Lee, B.A. Brunett, L. Franks, and R.B. James, *Mater. Sci. Eng.* **R32**, 103 (2001).

[2] Cs. Szeles, S.E. Cameron, S.A. Soldner, J.-O. Ndap, M.D. Reed, *J. Electron Mater.* **33**, 742 (2004).

[3] L. Li, F. Lu, C. Lee, G.W. Wright, D.R. Rhiger, S. Sen, K.S. Shah, M.R. Squillante, L.J. Cirignano, R.B. James, A. Burger, P.N. Luke, R. Olsen, *SPIE Proceedings Series*, Vol. **4787**, 76 (2003).

[4] Redlen Crystals (private communication).

[5] Cs. Szeles, W.C. Chalmers, S.C. Cameron, J.-O. Ndap, M. Bliss, and K.G. Lynn, *SPIE Proceedings Series*, Vol. **4507**, 57 (2001).

[6] M. Fiederle, V. Babentsov, J. Franc, A. Fauler, and J.-P. Konrath, *Cryst. Res. Technol.* **38**, 588 (2003).

[7] F. Zhang, Z. He D. Xu, G.F. Knoll, D.K. Wehe, J.E. Berry, *IEEE Trans Nucl. Sci.* **NS-51**, 2427 (2004).

[8] M. Amman, J.S. Lee, and P.N. Luke, *J. Appl. Phys.* **92**, 3198 (2002).

[9] D.S. Bale, Cs. Szeles and J. Grosholtz, Jr., these proceedings (Talk 6319A-12).

[10] Cs. Szeles, *IEEE Trans Nucl. Sci.* **51**, 1242 (2004).

[11] S.A. Soldner, A.J. Narvett, D.E. Covalt and Cs. Szeles, *IEEE Trans Nucl. Sci.* **51**, 2443 (2004).

[12] G.A. Carini, A.E. Bolotnikov, G.S. Camarda, G.W. Wright, L. Li, and R.B. James, *Appl. Phys. Lett.* **88**, 143515 (2006).

[13] M. Prokesch and Cs. Szeles, *J. Appl. Phys.* **100**, 14503 (2006).

[14] K. Hecht, *Zeits. Phys.* **77**, 235 (1932).

[15] S.P. McNeil, K.G. Lynn, M.H. Weber, Cs. Szeles, R. Soundararajan, *J. Electron Mater.* **32**, 583 (2003).

[16] A.E. Bolotnikov, G.S. Camarda, G.A. Carini, L. Li, and R.B. James, these proceedings (Talk 6319A-02).